Cellular/Molecular

AMIGO1 Promotes Axon Growth and Territory Matching in the Retina

Florentina Soto,[1] **Ning Shen,**[1] **and Daniel Kerschensteiner**[1,2,3,4]

[1]John F. Hardesty, MD, Department of Ophthalmology and Visual Sciences, Washington University School of Medicine, St. Louis, Missouri 63110, [2]Department of Neuroscience, Washington University School of Medicine, St. Louis, Missouri 63110, [3]Department of Biomedical Engineering, Washington University School of Medicine, St. Louis, Missouri 63110, and [4]Hope Center for Neurological Disorders, Washington University School of Medicine, St. Louis, Missouri 63110

Dendrite and axon arbor sizes are critical to neuronal function and vary widely between different neuron types. The relative dendrite and axon sizes of synaptic partners control signal convergence and divergence in neural circuits. The developmental mechanisms that determine cell-type-specific dendrite and axon size and match synaptic partners' arbor territories remain obscure. Here, we discover that retinal horizontal cells express the leucine-rich repeat domain cell adhesion molecule AMIGO1. Horizontal cells provide pathway-specific feedback to photoreceptors—horizontal cell axons to rods and horizontal cell dendrites to cones. AMIGO1 selectively expands the size of horizontal cell axons. When *Amigo1* is deleted in all or individual horizontal cells of either sex, their axon arbors shrink. By contrast, horizontal cell dendrites and synapse formation of horizontal cell axons and dendrites are unaffected by AMIGO1 removal. The dendrites of rod bipolar cells, which do not express AMIGO1, shrink in parallel with horizontal cell axons in *Amigo1 knockout* (*Amigo1 KO*) mice. This territory matching maintains the function of the rod bipolar pathway, preserving bipolar cell responses and retinal output signals in *Amigo1 KO* mice. We previously identified AMIGO2 as a scaling factor that constrains retinal neurite arbors. Our current results identify AMIGO1 as a scaling factor that expands retinal neurite arbors and reveal territory matching as a novel homeostatic mechanism. Territory matching interacts with other homeostatic mechanisms to stabilize the development of the rod bipolar pathway, which mediates vision near the threshold.

Key words: **arbor size; circuit development; horizontal cell; LRR protein; rod bipolar pathway**

Significance Statement

Neurons send and receive signals through branched axonal and dendritic arbors. The size of these arbors is critical to the function of a neuron. Axons and dendrites grow during development and are stable at maturity. The mechanisms that determine axon and dendrite size are not well understood. Here, we identify a cell surface protein, AMIGO1, that selectively promotes axon growth of horizontal cells, a retinal interneuron. Removal of AMIGO1 reduces the size of horizontal cell axons without affecting the size of their dendrites or the ability of both arbors to form connections. The changes in horizontal cell axons are matched by changes in synaptic partner dendrites to stabilize retinal function. This identifies territory matching as a novel homeostatic plasticity mechanism.

Introduction

Dendrite and axon arbor sizes are critical to neuronal function. Dendrite territories determine the position and number of inputs a neuron can recruit (i.e., the receptive field), whereas axon territories restrict the position and number of its output partners (i.e., the projective field; Lefebvre et al., 2015; Prigge and Kay, 2018). Dendrites and axons grow and remodel during development to attain specific sizes at maturity (Lefebvre et al., 2015; Prigge and Kay, 2018). Dendrite and axon sizes vary dramatically across neuron types (Brown et al., 2008). The molecular mechanisms that control the development of cell-type-specific dendrite and axon territories are mostly unknown.

Received June 5, 2021; revised Jan. 17, 2022; accepted Jan. 23, 2022.

Author contributions: F.S. and D.K. designed research; F.S. and N.S. performed research; F.S. and D.K. analyzed data; F.S. and D.K. wrote the paper.

This work was supported by the National Institutes of Health Grants EY027411 (F.S. and D.K.), EY023341 (D.K.), and EY026978 (D.K.); the Grace Nelson Lacy Research Fund (D.K.); and an unrestricted grant (Department of Ophthalmology and Visual Sciences) from Research to Prevent Blindness. We thank Dr. Nicholas Brecha and Dr. Rachel O. Wong, who provided the *Cx57-iCre* and *Gad1-GFP* mice, respectively.

The authors declare no competing financial interests.

Correspondence should be addressed to Florentina Soto at sotof@wustl.edu or Daniel Kerschensteiner at dkerschensteiner@wustl.edu.

https://doi.org/10.1523/JNEUROSCI.1164-21.2022

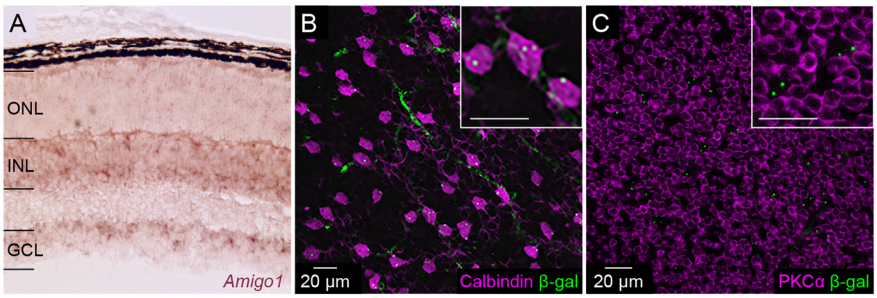

Figure 1. Horizontal cells express *Amigo1*. ***A***, *In situ* hybridization detects *Amigo1* mRNA in a band of evenly space neurons at the outer margin of the inner nuclear layer (INL). Additional expression is observed deeper in the INL and in the ganglion cell layer (GCL). ***B***, ***C***, Immunohistochemistry for β-galactosidase (β-gal) expressed from the *Amigo1* locus in retinal flat mounts, costained for calbindin (***B***) and PKCα (***C***), which label horizontal and rod bipolar cells, respectively. The elongated labeling in the β-gal channel (***B***) represents blood vessels stained by the secondary anti-mouse-IgG antibody. Insets (***B***, ***C***) show magnified views. Scale bars: 20 µm.

The first three interneurons of the visual system (i.e., retinal horizontal and amacrine cells and thalamic local interneurons) have bifunctional neurites that receive input and provide output (Diamond, 2017; Morgan and Lichtman, 2020). The respective neurite arbors process visual information locally, increasing spatial resolution and allowing one neuron to participate separately in different circuits (Nelson et al., 1975; Euler et al., 2002; Grimes et al., 2010; Crandall and Cox, 2012; Chapot et al., 2017; Hsiang et al., 2017). Horizontal cells elaborate two bifunctional neurite arbors; their axons receive input from rod photoreceptors (or rods), send feedback to rods, and feedforward signals to rod bipolar cells, whereas their dendrites receive input from cone photoreceptors (or cones), send feedback to cones, and feedforward signals to cone bipolar cells (Thoreson and Mangel, 2012; Diamond, 2017). Horizontal cell axons and dendrites are electrotonically separated and participate largely independently in rod- and cone-mediated vision, respectively (Nelson et al., 1975; Trümpler et al., 2008; Szikra et al., 2014). How horizontal cells, or other neurons, regulate the growth of different neurites in a pathway-specific manner is unclear.

The function of a neural circuit depends on the ratio in which its cellular components are combined, which, in turn, depends on the relative arbor sizes of synaptic partners (Sinha et al., 2017; Soto et al., 2019). How arbor sizes are matched between synaptic partners to establish and stabilize circuit function is unknown.

Here, we discover that developing retinal horizontal cells express the homophilic cell adhesion molecule AMIGO1. When *Amigo1* is deleted in all (*Amigo1 KO* mice) or a few (*AAV-CRISPR*) horizontal cells, their axon but not dendrite growth is stunted. Deficits are selective to arbor growth, whereas synapse formation is unaffected by AMIGO1 removal. Changes in horizontal cell axon growth are matched by rod bipolar cell dendrite growth changes, preserving retinal function in dim light. Our results identify AMIGO1 as a neurite scaling factor that matches the arbor territories of synaptic partners.

Territory matching is predicted to stabilize circuit function. Consistent with this prediction, we find that rod bipolar cell responses and ganglion cell spike trains elicited by dim and bright light stimuli (i.e., the retinal output) are precisely preserved in *Amigo1 KO* mice (see Figs. 8, 10). This adds territory matching to a series of homeostatic mechanisms that maintain the function of the rod bipolar pathway, underscoring the evolutionary pressure on the function of this pathway (Sher et al., 2013; Johnson et al., 2017; Care et al., 2020; Leinonen et al., 2020).

Materials and Methods

Animals. We rederived *Amigo1 KO* (*Amigo1*$^{tm1.1(KOMP)Vlcg}$/*JMmucd*) mice from embryonic stem (ES) cell clone 10669A-E11, obtained from the KOMP Repository (www.komp.org) and generated by Regeneron Pharmaceuticals (Valenzuela et al., 2003). In these mice, homology arms were used to target the sequence upstream of the ATG initiation codon (5′ arm) and downstream of the TAG termination codon (3′ arm). Thus, the whole coding sequence of *Amigo1* was removed with a 1476 bp deletion from 107990108-107991583 on chromosome 3 (Genome Build37) and replaced with a *lacZ* reporter (i.e., the gene encoding β-galactosidase) and a floxed selection marker (i.e., Neomycin). In our ES cell clone, the Neomycin cassette had been excised. Therefore, *Amigo1 KO* mice express β-galactosidase from the *Amigo1* locus and produce no truncated AMIGO1 protein. We genotyped these mice with *Amigo1*-specific oligos for the wild-type allele (Forward: 5'-CAT CTT CAC ACG CTG GAT GAG TTC C-3′ and Reverse: 5′-TCC CAT CCT TGA TCA GTT CCA CAG G-3′) and *lacZ*-specific oligos for the *Amigo1 KO* allele (Forward: 5′-GTT GCA GTG CAC GGC AGA TAC ACT TGC TGA-3′ and Reverse: 5′-GCC ACT GGT GTG GGC CAT AAT TCA ATC GC-3′) to generate PCR products of 184 bp (wild type) and 389 bp (*Amigo1 KO*), respectively. The PCR steps were the following: (1) 94°C for 2 min, (2) cycle 35 times between 94° for 30 s and 68° for 2 min, and (3) extension at 68°C for 7 min. The PCR was catalyzed by KlenTaq LA (catalog #110, DNA Polymerase Technology). We previously generated *Amigo2 KO* mice using transcription activator-like effector nucleases (TALENs; Soto et al., 2019). We crossed *Gad1-GFP* mice to *Amigo1 KO* to visualize developing horizontal cells (Chattopadhyaya et al., 2004; Huckfeldt et al., 2009). We crossed *Cx57-iCre* (Hirano et al., 2016) and *R26-LSL-Cas9* (Platt et al., 2014) to generate mice in which horizontal cells express the RNA-guided DNA endonuclease Cas9. We used male and female *Amigo1 KO*, *Amigo1 KO Gad1-GFP*, *Amigo1 Amigo2 double KO* (*DKO*), *Cx57-iCre R26-LSL-Cas9*, and littermate wild-type mice throughout this study. We analyzed male and female mice separately but subsequently combined their data because we observed no sex-specific differences. All procedures in this study were approved by the Animal Studies Committee of Washington University School of Medicine (Protocol no. 20–0055) and performed in compliance with the National Institutes of Health *Guide for the Care and Use of Laboratory Animals*.

Adeno-associated viruses. To label horizontal cells and rod bipolar cells, we injected 250 nl of *AAV2/1-CAG-YFP* (Soto et al., 2018) and *AAV2/1-Grm6-tdTomato* (Johnson et al., 2017), respectively, into the vitreous of newborn wild-type and *Amigo1 KO* mice via a Nanoject II injector (Drummond). To delete *Amigo1* in a sparse horizontal cell subset, we tested two sgRNAs against *Amigo1* in cultured Cas9-expressing fibroblasts. We selected the one that generated insertion and deletion mutations (indels) with higher efficiency (>80%) to produce *AAV2/1-U6-sgAmigo1-CAG-tdTomato*. We then injected 250 nl of *AAV2/1-U6-sgAmigo1-CAG-tdTomato* into the vitreous of *Cx57-iCre R26-LSL-Cas9* mice and Cre-negative littermates.

In vivo *electroporation.* To sparsely label rods, we injected *pNrl-EGFP* plasmid into the subretinal space of newborn mice anesthetized on ice via a Nanoject II injector (Drummond). We delivered five 80 V square pulses of 50 ms duration generated by an ECM 830 (BTX, Harvard Apparatus) via tweezer electrodes with the anode placed on the injected eye to electroporate rods (Matsuda and Cepko, 2007, 2008).

In vivo *electroretinography.* Mice were dark adapted overnight, anesthetized with ketamine (0.1 mg/g body weight) and xylazine (0.01 mg/g body weight), and their pupils dilated with 1% atropine sulfate (Falcon Pharmaceuticals). We recorded responses to brief (<5 ms) white light flashes in control, *Amigo1 KO*, and *Amigo1 Amigo2 DKO* mice using a UTAS Visual Electrodiagnostic Testing System (LKC Technologies). Recording electrodes embedded in contact lenses were placed over the

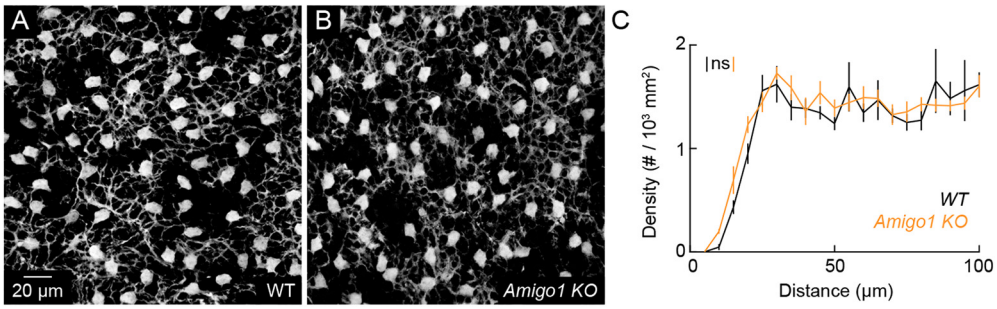

Figure 2. Horizontal cell mosaics are unchanged in *Amigo1 KO* retinas. ***A***, ***B***, Representative images of horizontal cell distributions in retina flat mounts from wild-type (***A***) and *Amigo1 KO* (***B***) littermates stained for calbindin. ***C***, Density recovery profiles of horizontal cells in wild-type and *Amigo1 KO* mice ($p = 0.53$, bootstrapping).

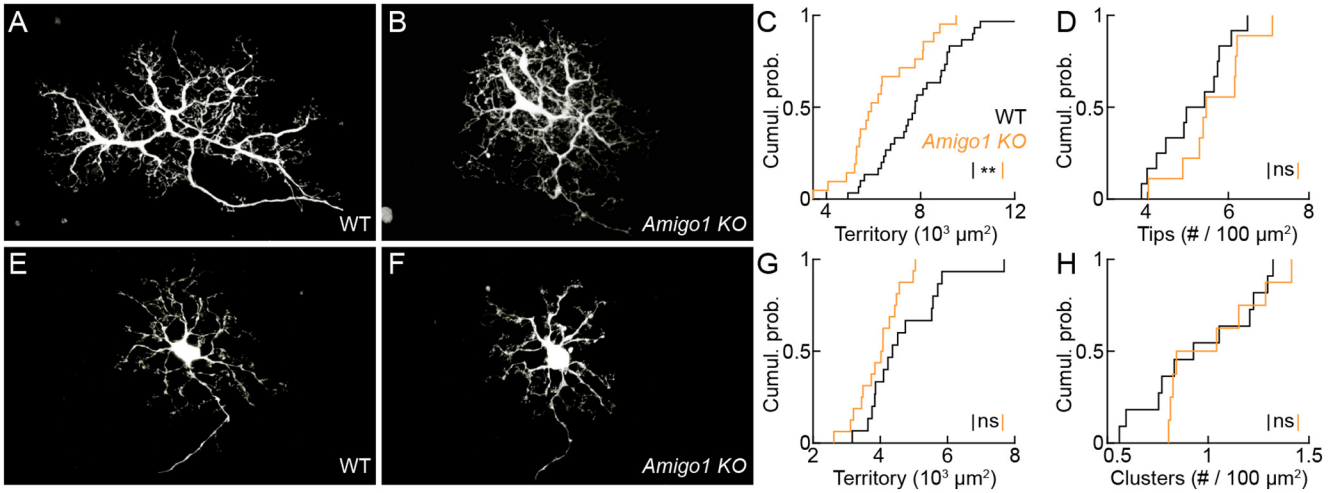

Figure 3. AMIGO1 promotes horizontal cell axon growth. ***A***, ***B***, Representative axon arbors of horizontal cells labeled by *AAV-CAG-YFP* in wild-type (***A***) and *Amigo1 KO* (***B***) retinas. ***C***, ***D***, Cumulative probability distributions of axon territories (***C***, wild type, $n = 30$; *Amigo1 KO*, $n = 21$; $p = 0.0026$, Mann–Whitney *U* test) and axon tip densities (***D***, wild type, $n = 12$; *Amigo1 KO*, $n = 9$; $p = 0.27$, Mann–Whitney *U* test). ***E***, ***F***, Representative dendrite arbors of horizontal cells labeled by *AAV-CAG-YFP* in wild-type (***E***) and *Amigo1 KO* (***F***) retinas. ***G***, ***H***, Cumulative probability distributions of dendrite territories (***G***, wild type, $n = 15$; *Amigo1 KO*, $n = 16$; $p = 0.086$, Mann–Whitney *U* test) and dendrite clusters densities (i.e., contacts with cones, ***H***; wild type, $n = 11$; *Amigo1 KO*, $n = 8$; $p = 0.66$, Mann–Whitney *U test*). ns indicates $p \geq 0.05$ and ** indicates $p < 0.01$.

cornea of both eyes. The mouse body temperature was maintained at 37 ± 0.5°C throughout recordings with a heating pad controlled by a rectal temperature probe (FHC). Flash electroretinographic (ERG) recordings were performed as previously described (Soto et al., 2013). We averaged 4 to 10 responses at each light level, measured the a-wave as the difference between the response minimum in the first 50 ms after flash onset and the voltage value at flash onset, and the b-wave as the difference between a 15–25 Hz low-pass-filtered b-wave peak and the a-wave amplitude. We performed flicker ERG recordings as previously described (Shen et al., 2020). Responses to trains of brief flashes at 2.53 cdS/m^2 with varying rates (5, 7, 10, 12, 15, 18, 20, and 30 Hz) were acquired without any background illumination. Responses to flicker stimuli were mean subtracted with a sliding window equal to one stimulus interval and averaged across 30 repeats before amplitudes were measured. All ERG analyses were performed using scripts written in MATLAB (MathWorks).

Tissue preparation. We killed mice with CO_2 and removed their eyes. For *in situ* hybridization, immunohistochemistry, and biolistic labeling, eyes were transferred into oxygenated mouse artificial cerebrospinal fluid ($mACSF_{HEPES}$) containing the following (in mM): 119 NaCl, 2.5 KCl, 1 NaH_2PO_4, 2.5 $CaCl_2$, 1.3 $MgCl_2$, 20 HEPES, and 11 glucose (pH adjusted to 7.37 using NaOH). Retinas were either isolated and flat mounted on filter paper (catalog #HABG01300, Millipore) or left in the eyecup for 30 min fixation with 4% paraformaldehyde in $mACSF_{HEPES}$. For multielectrode array recordings, mice were dark adapted for >2 h before their retinas were isolated under infrared illumination (>900 nm) in $mACSF_{NaHCO3}$ containing the following (in mM): 125 NaCl, 2.5 KCl, 1 $MgCl_2$, 1.25 NaH_2PO_4, 2 $CaCl_2$, 20 glucose, 26 $NaHCO_3$ and 0.5 L-glutamine equilibrated with 95% O_2/5% CO_2.

In situ *hybridization.* We followed previously described *in situ* hybridization methods (Soto et al., 2013, 2019). We prepared the DNA template for riboprobes by PCR from a Mammalian Gene Collection clone obtained from Dharmacon/Horizon Discovery using the following primers: T3 sense: 5′-GCAATTAACCCTCACTAAAGCAGGGCCG GCCGATCTGTGGTTAGT-3′ and T7 antisense: 5′-TAATACGCA TCACTATAGGTGGTCATGCCTTGCTGTTTGGTGT-3′. We synthesized the antisense RNA probes using the DIG RNA labeling kit (Roche) from T7 sites incorporated by PCR in the DNA template. Fixed eyecups (see Tissue preparation) were cryoprotected and sliced (thickness: 20 µm) with a cryotome (Leica). Retinal sections were pretreated using proteinase K, postfixed, permeabilized using Triton X-100, and prehybridized for 4 h at 65°C. Hybridization was performed overnight at 65°C using 1–2 µg/ml antisense RNA. The hybridized riboprobe was detected using anti-DIG alkaline phosphatase labeled antibodies and NBT/BCIP (Roche) overnight.

Immunohistochemistry. Vibratome slices (thickness 60 µm) were blocked for 2 h with 5% normal donkey serum in PBS, embedded in 4% agarose (Sigma), and incubated overnight at 4°C with primary antibodies. Slices were then washed in PBS (3 × 20 min) and incubated in secondary antibodies for 2 h. Flat-mount preparations were frozen and thawed three times after cryoprotection (1 h 10% sucrose in PBS, 1 h 20% sucrose in PBS, and overnight 30% sucrose in PBS at 4°C), blocked with 5% normal donkey serum in PBS for 2 h, and then incubated with primary antibodies for 5 d at 4°C and washed in PBS (3 × 1 h).

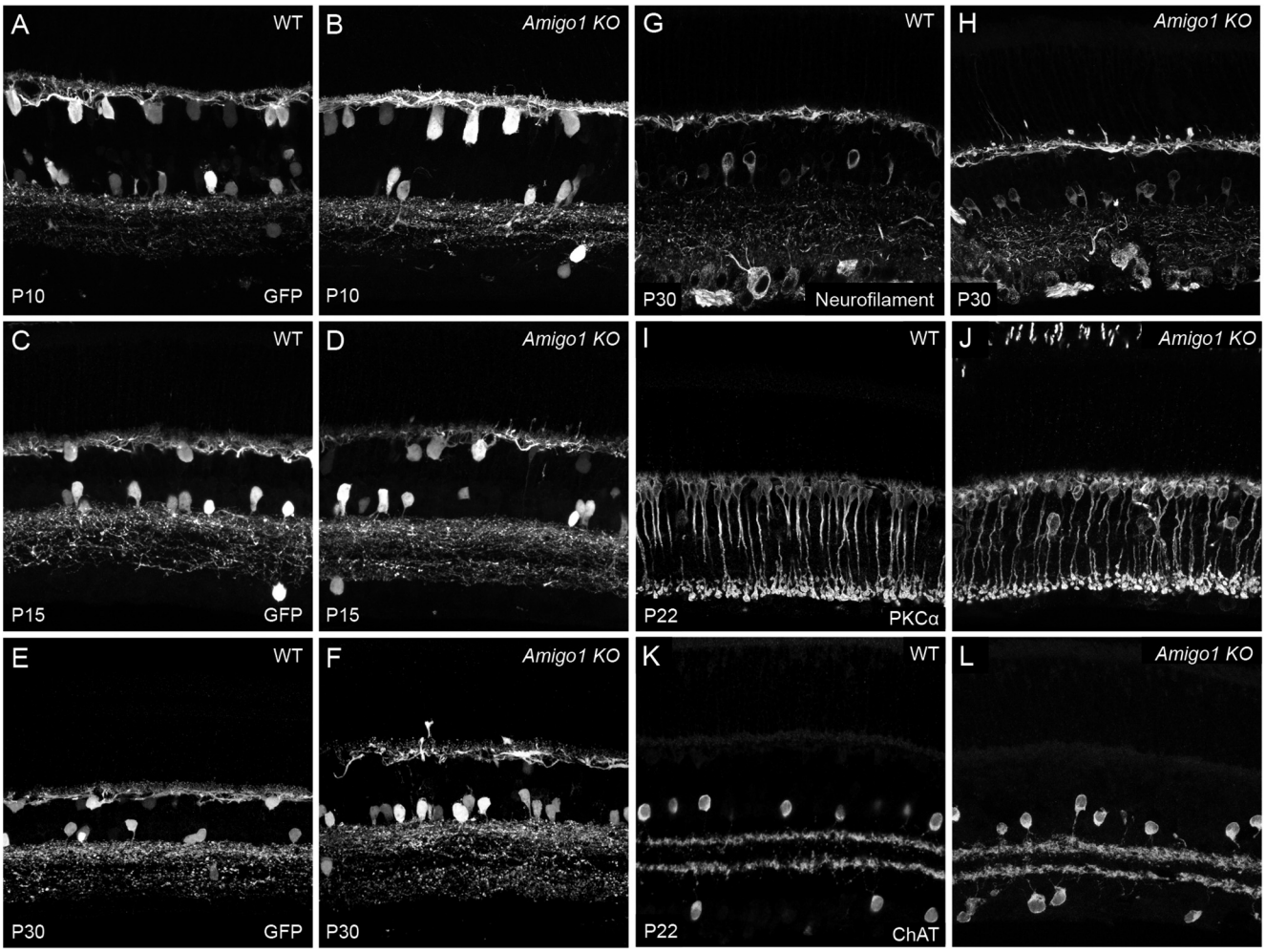

Figure 4. Targeting errors of horizontal cell axons but not other neurites in *Amigo1 KO* retinas. ***A–F***, Representative images of retinal vibratome slices from P10 (***A***, ***B***), P15 (***C***, ***D***), and P30 (***E***, ***F***) *Amigo1* wild-type *Gad1-GFP* (***A***, ***C***, ***E***) and *Amigo1 KO Gad1-GFP* mice (***B***, ***D***, ***F***). ***G***, ***H***, Representative images of vibratome slices of P30 wild-type (***G***) and *Amigo1 KO* (***H***) retinas stained for neurofilament show that the mistargeted horizontal cell neurites in the outer nuclear layer are axons. ***I***, ***J***, Representative images of retinal vibratome slices from P22 wild-type (***I***) and *Amigo1 KO* (***J***) mice, stained for the rod bipolar cell marker PKCα. Rod bipolar cell dendrites do not make the same targeting errors as horizontal cell axons. ***K***, ***L***, Representative images of retinal vibratome slices from wild-type (***K***) and *Amigo1 KO* (***L***) mice stained for choline acetyltransferase to label starburst amacrine cells.

Subsequently, flat mounts were incubated with secondary antibodies for 1 d at 4°C and washed in PBS (3 × 1 h). The following primary antibodies were used in this study: mouse anti-Bassoon (1:500; catalog #SAP7F407, Enzo Life Sciences; RRID:AB_2313990), mouse anti-β-galactosidase (1:200; Developmental Studies Hybridoma Bank clone 40-1a, deposited by J.R. Sanes), mouse anti-CACNA1S (1:500; catalog #MAB427, Millipore; RRID:AB_2069582) to label GPR179 (Hasan et al., 2016), rabbit anti-DsRed (1:1000; catalog #632496, Takara Bio; RRID:AB_10013483), mouse anti-Calbindin (1:1000; catalog #214 011C3, Synaptic Systems; RRID:AB_2619898), rabbit anti-GFP (1:1000; ThermoFisher), and mouse anti-PKCα (1:500; catalog #P5704, Sigma-Aldrich; RRID:AB_477375). Secondary antibodies were Alexa 488 and Alexa 568 conjugates (1:1000; Invitrogen).

Confocal imaging and analysis. Image stacks were acquired on an FV1000 confocal laser-scanning microscope (Olympus) using a 60 × 1.35 NA oil-immersion objective at a voxel size of 0.103–0.3 μm (x/y – z), 0.206–0.3 μm or 0.069–0.3 μm or on an LSM 800 with Airyscan detectors (Zeiss) using a 63 × 1.4 NA objective at a voxel size of 0.04–0.15 μm. Image volumes were processed in Amira (Thermo Fisher) and ImageJ/Fiji (http://rsbweb.nih.gov/ij; Schindelin et al., 2012) and analyzed using custom scripts written in MATLAB (MathWorks) and Python (Van Rossum and Drake, 2009).

To analyze the volume of rod terminals, they were masked in WT and KO animals in image stacks of retinal flat-mount preparations from mice that have rods labeled using *pNrl-EGFP* and their volume calculated using the material statistics function of Amira. Horizontal and rod bipolar cell axon and dendrite territories were defined as the areas of the smallest convex polygons to encompass the respective arbors in z-projections of confocal image stacks acquired in retinal flat mounts. To assess the density of horizontal cell axon branches, we used minimum cross-entropy thresholding to measure the territory of each horizontal cell axon occupied by branches (Li and Lee, 1993). Horizontal cell dendrite clusters at cone terminals and horizontal cell axon tips, which penetrate rod spherules, were identified by eye in confocal image stacks, and their positions (x, y, and z) were noted. The same procedure was used to count synapses on the tips of rod bipolar cell dendrites that were stained for GPR179.

Multielectrode array recordings and analysis. We recorded ganglion cells on planar 252-electrode arrays (30 µm electrode size, 100 µm center-center spacing, Multi Channel Systems). Retinas were perfused with warm (30–33°C) $mACSF_{NaHCO3}$ equilibrated with 95% O_2/5% CO_2 at 5–7 ml/min. The electrode signals were bandpass filtered (300–3000 Hz) and digitized at 10 kHz. Signal cutouts from 1 ms before to 2 ms after crossings of negative thresholds (set manually for each channel) were recorded to hard disk together with the time of threshold crossing (i.e., the spike time). We sorted spikes into trains representing the activity of individual neurons by principal component analysis of spike waveforms (Offline Sorter, Plexon) and used refractory periods to assess the quality

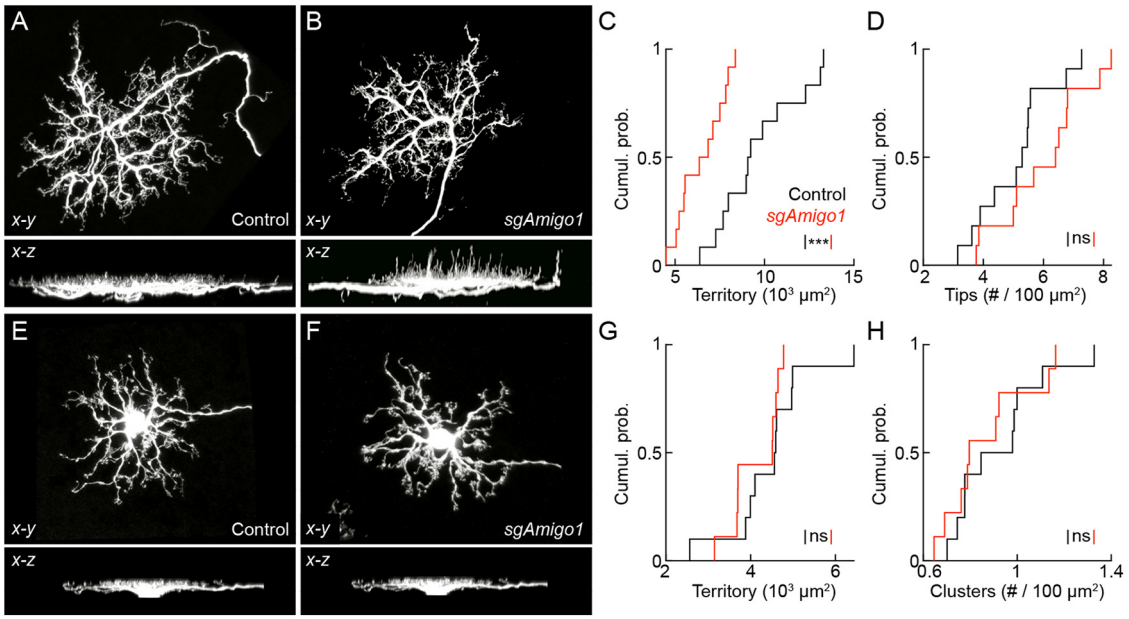

Figure 5. AMIGO1 transmits signals for axon growth and laminar targeting. ***A***, ***B***, Orthogonal views of representative axon arbors of horizontal cells infected with *AAV2/1-U6-sgAmigo1-CAG-tdTomato* in *Cx57-iCre R26-LSL-Cas9* mice (***B***) and Cre-negative control littermates (***A***). ***C***, ***D***, Cumulative probability distributions of axon territories (***C***, Control, $n = 12$; *sgAmigo1*, $n = 12$; $p = 9 \times 10^{-4}$, Mann–Whitney *U* test) and axon tip densities in the outer plexiform layer (***D***, Control, $n = 12$; *sgAmigo1*, $n = 12$; $p = 0.17$, Mann–Whitney *U* test). ***E***, ***F***, Orthogonal views of dendrite arbors of horizontal cells infected with *AAV2/1-U6-sgAmigo1-CAG-tdTomato* in *Cx57-iCre R26-LSL-Cas9* mice (***F***) and Cre-negative control littermates (***E***). ***G***, ***H***, Cumulative probability distributions of dendrite territories (***G***, Control, $n = 10$; *sgAmigo1*, $n = 9$; $p = 0.32$, Mann–Whitney *U* test) and dendrite clusters densities (i.e., contacts with cones; ***H***, Control, $n = 10$; *sgAmigo1*, $n = 9$; $p = 0.60$, Mann–Whitney *U* test). ns indicates $p \geq 0.05$ and *** indicates $p < 0.001$.

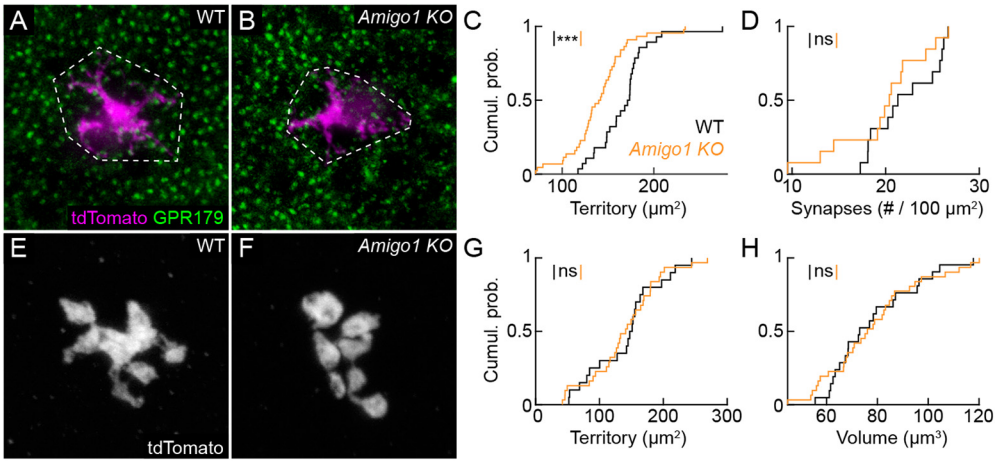

Figure 6. Territory matching of rod bipolar cell dendrites in *Amigo1 KO* mice. ***A***, ***B***, Representative images of rod bipolar cell dendrites (labeled by *AAV-Grm6-tdTomato*) and postsynaptic sites (stained for GPR179) in wild-type (***A***) and *Amigo1 KO* (***B***) retinas. Cumulative probability distributions of rod bipolar cell dendrite territories (***C***, wild type, $n = 28$; *Amigo1 KO*, $n = 44$; $p = 2.1 \times 10^{-4}$, Mann–Whitney *U* test) and synapse densities (***D***, wild type, $n = 13$; *Amigo1 KO*, $n = 13$; $p = 0.36$, Mann–Whitney *U* test). ***E***, ***F***, Representative images of rod bipolar cell axons (labeled by *AAV-Grm6-tdTomato*) in wild-type (***E***) and *Amigo1 KO* (***F***) retinas. ***G***, ***H***, Cumulative probability distributions of rod bipolar cell axon territories (***G***, wild type, $n = 20$; *Amigo1 KO*, $n = 31$; $p = 0.82$, Mann–Whitney *U* test) and volumes (***H***, wild type, $n = 21$; *Amigo1 KO*, $n = 31$; $p = 0.96$, Mann–Whitney *U* test). ns indicates $p \geq 0.05$ and *** indicates $p < 0.001$.

of the sorting, retaining only spike trains in which <0.2% of interspike intervals were <2 ms. When the activity of a single neuron had been recorded on more than one electrode (identified by cross-correlation), we used only the train with the most spikes in our subsequent analysis.

Light stimuli were presented on an organic light-emitting display (OLED-XL, eMagin) and focused onto the retina through a 20 × 0.5 NA water immersion objective (Olympus). Stimuli were generated in MATLAB using the Cogent Graphics toolbox extensions developed by John Romaya at the Laboratory of Neurobiology at the Wellcome Department of Imaging Neuroscience. The display output was linearized with custom-written scripts. We analyzed luminance contrast encoding of ganglion cells with linear-nonlinear (LN) models constructed from responses to Gaussian white noise stimuli (Chichilnisky, 2001; Soto et al., 2020). The display was divided into vertical bars (width, 50 µm; height, 1.7 mm). The intensity of each bar was chosen at random every 33 ms (refresh rate: 30 Hz) from a Gaussian distribution (RMS contrast, 40%) for 30 min. At 50 s intervals, a 10 s segment of white noise was repeated. The average intensity was 10 rhodopsin isomerizations/rod/s (R*) for scotopic stimuli and 1000 R* for photopic stimuli. Spatiotemporal receptive fields (i.e., the linear component of the LN models) were mapped by computing spike-triggered stimulus averages (STA) from a nonrepeating part of the Gaussian white

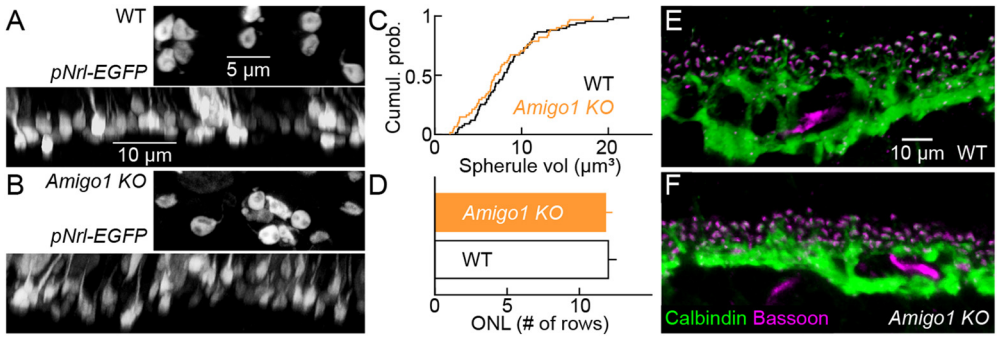

Figure 7. Rods develop independently of AMIGO1. ***A***, ***B***, Representative top-down (top) and side views (bottom) of rod spherules labeled by *in vivo* electroporation of *pNrl-EGFP* in wild-type (***A***) and *Amigo1 KO* mice (***B***). Top, Magnified excerpts from the regions shown in the side views. ***C***, Cumulative probability distributions of rod spherule volumes (wild type, $n = 67$; *Amigo1 KO*, $n = 61$; $p = 0.37$, Mann–Whitney *U* test). ***D***, Error bars indicate the mean (± SEM) number of rows in the outer nuclear layer measure in DAPI-stained sections (wild type, $n = 3$ retinas; *Amigo1 KO*, $n = 5$ retinas; $p = 0.93$, Mann–Whitney *U* test). ***E***, ***F***, Representative images of retinal vibratome slices from wild-type (***E***) and *Amigo1 KO* (***F***) mice showing the outer plexiform layer stained for calbindin, a horizontal cell marker, and Bassoon, a presynaptic ribbon-anchoring protein.

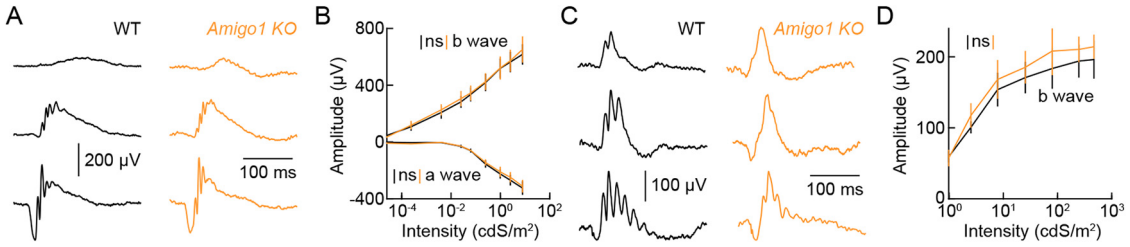

Figure 8. Electroretinographic responses are preserved in *Amigo1 KO* mice. ***A***, Representative ERG responses of dark-adapted wild-type (left) and *Amigo1 KO* (right) mice to flashes of increasing intensity (top, 2.4×10^{-4} cdS/m^2; middle, 0.025 cdS/m^2; bottom, 0.98 cdS/m^2). ***B***, Population data (mean ± SEM) of dark-adapted a-wave amplitudes (wild type, $n = 6$ mice; *Amigo1 KO*, $n = 5$ mice; $p = 0.83$, bootstrapping) and b-wave amplitudes ($p = 0.94$, bootstrapping). ***C***, Representative ERG responses of light-adapted wild-type (left) and *Amigo1 KO* (right) mice to flashes of increasing intensity (top, 2.5 cdS/m^2; middle, 26 cdS/m^2; bottom, 470 cdS/m^2). ***D***, Population data (mean ± SEM) of the light-adapted b-wave amplitudes (wild type, $n = 5$ mice; *Amigo1 KO*, $n = 5$ mice; $p = 0.68$, bootstrapping). ns indicates $p \geq 0.05$.

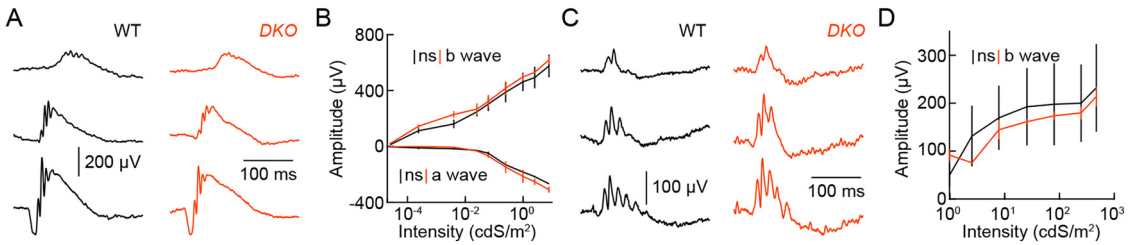

Figure 9. Electroretinographic responses are preserved in *Amigo1 Amigo2 double knockout* mice. ***A***, Representative ERG responses of dark-adapted wild-type (left) and *Amigo1 Amigo2 DKO* (right) mice to flashes of increasing intensity (top, 2.4×10^{-4} cdS/m^2; middle, 0.025 cdS/m^2; bottom, 0.98 cdS/m^2). ***B***, Population data (mean ± SEM) of dark-adapted a-wave amplitudes (wild type, $n = 3$ mice; *DKO*, $n = 3$ mice; $p = 0.26$, bootstrapping) and b-wave amplitudes ($p = 0.56$, bootstrapping). ***C***, Representative ERG responses of light-adapted wild-type (left) and *DKO* (right) mice to flashes of increasing intensity (top, 2.5 cdS/m^2; middle, 26 cdS/m^2; bottom, 470 cdS/m^2). ***D***, Population data (mean ± SEM) of the light-adapted b-wave amplitudes (wild type, $n = 3$ mice; *DKO*, $n = 3$ mice; $p = 0.55$, bootstrapping). ns indicates $p \geq 0.05$.

noise. A separate nonrepeating part of the stimulus was convolved with the STA to calculate a vector of generator signals and estimate contrast-response functions. At each time point, the generator signal describes the match between the spatiotemporal receptive field and the preceding stimulus (i.e., the effective stimulus contrast). The dependence of the firing rate on the generator signal was fit with a sigmoidal function (i.e., the nonlinear component of the LN models) as follows:

$$r(g) = \alpha C(\beta g - \gamma) + \delta,$$

where $r(g)$ is the firing rate as a function of the generator signal, C is the cumulative normal distribution function, and α, β, γ, and δ are free parameters. To compare temporal receptive fields of different ganglion cells, we calculated the time to peak sensitivity (i.e., time to peak), the time to the subsequent zero crossing (i.e., time to zero), and a biphasic index (bi) as follows:

$$bi = 1 - \frac{|peak + trough|}{|peak| + |trough|},$$

where peak and trough refer to the maximum and minimum of the temporal filter, respectively. To estimate receptive field sizes, we calculated the variance of different bars across the time of the STA and fit a Gaussian function to the result. The receptive field size was defined as 1 SD of the Gaussian. To compare contrast-response functions, we computed their nonlinearity as the logarithm of the ratio of the slope at the response maximum to the slope of the response at generator signal = 0, their gain as the logarithm of the slope at generator signal = 0, and their threshold as a

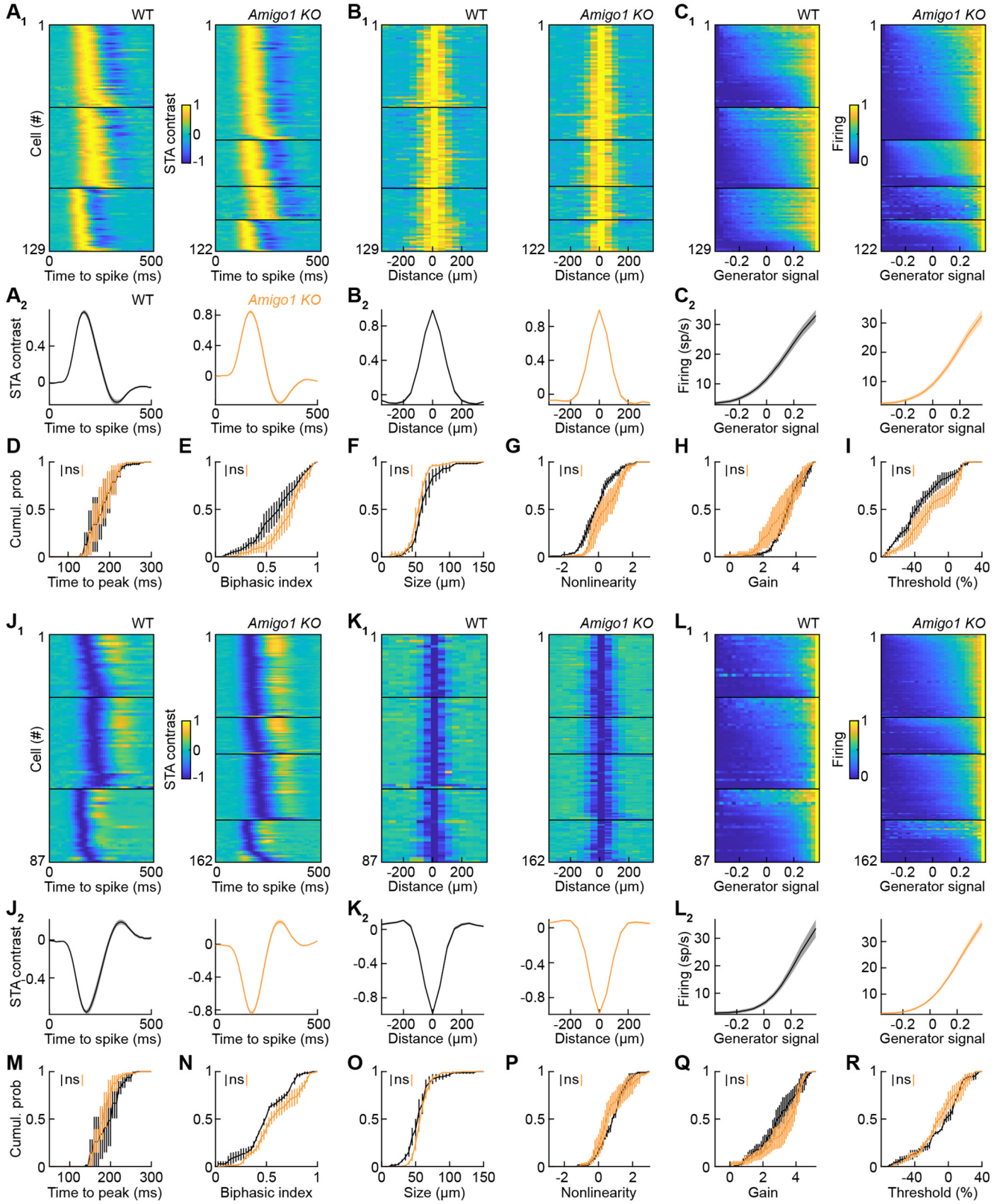

Figure 10. Homeostasis of dim-light visual processing in *Amigo1 KO* retinas. ***A***, Temporal receptive fields of all ON ganglion cells recorded in wild-type (***A*$_1$**, left, $n = 129$ cells, $n = 3$ mice) and *Amigo1 KO* (***A*$_1$**, right, $n = 122$ cells, $n = 4$ mice) retinas, grouped by mice, sorted by time to peak, and their averages (***A*$_2$**, ± SEM). ***B***, Spatial receptive fields of all ON ganglion cells recorded in wild-type (***B*$_1$**, left) and *Amigo1 KO* (***B*$_1$**, right) retinas, grouped by mice, sorted by size, and their averages (***B*$_2$**, ± SEM). ***C***, Static nonlinearities (or effective-contrast-response functions) of all ON ganglion cells recorded in wild-type (***C*$_1$**, left) and *Amigo1 KO* (***C*$_1$**, right) retinas, grouped by mice, sorted by threshold, and their averages (***C*$_2$**, ± SEM). ***D–I***, Cumulative probability distributions of the time to peak (***D***, wild type vs *Amigo 1KO*, $p = 0.89$, bootstrapping) and biphasic index (***E***, $p = 0.14$, bootstrapping) of temporal receptive fields, size of spatial receptive fields (***F***, $p = 0.22$, bootstrapping), and the nonlinearity (***G***, $p = 0.14$, bootstrapping), gain (***H***, $p = 0.44$, bootstrapping), and threshold (***I***, $p = 0.15$, bootstrapping) of the effective-contrast-response functions. ***J***, Temporal receptive fields of all OFF ganglion cells recorded in wild-type (***J*$_1$**, left, $n = 87$ cells, $n = 3$ mice) and *Amigo1 KO* (***J*$_1$**, right, $n = 162$ cells, $n = 4$ mice) retinas, grouped by mice, sorted by time to peak, and their averages (***J*$_2$**, ± SEM). ***K***, Spatial receptive fields of all OFF ganglion cells recorded in wild-type (***K*$_1$**, left) and *Amigo1 KO* (***K*$_1$**, right)

percentage of the range of effective stimulus contrasts (−100% to 100%) at which the response reaches 10% of its maximum (Pearson and Kerschensteiner, 2015; Soto et al., 2020).

Experimental design and statistical analysis. Mann–Whitney *U* tests were used to assess the statistical significance of differences between single-parameter characteristics (e.g., axon territories) of experimental groups, except for categorical variables (e.g., β-gal positive and negative), which were compared by χ^2 tests. Continuous relationships with multiple measurements (e.g., contrast-response functions) were compared by bootstrapping with 10,000 replicates. Results were considered significant if $p < 0.05$. The following asterisks were used to indicate significance levels in the figures: $^*p < 0.05$, $^{**}p < 0.01$, and $^{***}p < 0.001$.

Results

Horizontal cells express *Amigo1*

We identified *Amigo1* in a screen for genes whose expression is upregulated in the inner nuclear layer during retinal circuit formation (Soto et al., 2013). *In situ* hybridization detected *Amigo1* mRNA in a sparse population of neurons at the outer margin of the inner nuclear layer in addition to cells deeper in the inner nuclear layer and the ganglion cell layer (Fig. 1*A*). *Amigo1* encodes a leucine-rich repeat (LRR) domain protein (AMIGO1) that belongs to a family of three homophilically interacting cell adhesion molecules (Kuja-Panula et al., 2003). To identify the cell type expressing *Amigo1* in the outer part of the inner nuclear layer, we combined β-galactosidase, staining from the *Amigo1 KO* allele with staining for calbindin and PKCα, markers of horizontal and rod bipolar cells, respectively (Fig. 1*B*,*C*). We found β-galactosidase puncta in nearly all calbindin-positive (223/242, $n = 4$ retinas) and almost no PKCα-positive cells (2/1188, $n = 3$ retinas, $p = 0$, χ^2 test), indicating that horizontal but not rod bipolar cells express *Amigo1*.

Horizontal cell mosaics are preserved in *Amigo1 KO* mice

To analyze how AMIGO1 shapes horizontal cell development, we rederived *Amigo1 KO* mice (Valenzuela et al., 2003). Retinal neurons are regularly spaced in cell-type-specific mosaics that distribute their computational functions evenly across visual space (Reese and Keeley, 2015; Kerschensteiner, 2020). We stained retinal flat-mount preparations from adult postnatal day (P)30 *Amigo1 KO* mice and wild-type littermates for calbindin to analyze the distributions of horizontal cells. Our results showed that the average density and density recovery profiles (Rodieck, 1991) of horizontal cells are indistinguishable between *Amigo1 KO* and wild-type mice, indicating that horizontal cells are born, survive, and form mosaics independently of AMIGO1 (Fig. 2*A*–*C*).

AMIGO1 promotes horizontal cell axon growth

To assess the contributions of AMIGO1 to neurite growth and connectivity, we sparsely labeled horizontal cells with *AAV-CAG-YFP* (Soto et al., 2013, 2018). Horizontal cell axons were significantly smaller in *Amigo1 KO* than wild-type mice (Fig. 3*A*–*C*), whereas horizontal cell dendrites were unaffected by the removal of AMIGO1 (Fig. 3*E*–*G*). The densities of horizontal cell axon tips and dendrite clusters, which penetrate rod spherules and cone pedicles, respectively, were unchanged by *Amigo1* deletion (Fig. 3*D*,*H*) as was the density of axon branches (i.e., fraction of the arbor territory occupied by branches; wild type, 26.0 ± 1.1%, $n = 26$; *Amigo1 KO*, 25.2 ± 1.2%; $n = 21$, $p = 1$, Mann–Whitney *U* test). Thus, AMIGO1 selectively promotes the growth of horizontal cell axons, not dendrites, and regulates arbor size independent of connectivity.

To visualize neurite targeting of developing horizontal cells, we crossed *Gad1-GFP* to *Amigo1 KO* mice (Chattopadhyaya et al., 2004; Huckfeldt et al., 2009). We observed sparse overshoots of horizontal cell processes into the outer nuclear layer in *Amigo1 KO* (*Gad1-GFP*) but not wild-type (*Gad1-GFP*) littermates. The mistargeted neurites were present from P10 (Fig. 4*A*–*F*) and stained for neurofilament (Fig. 4*G*,*H*), indicating that in the absence of AMIGO1, developing horizontal cell axons make errors in laminar targeting. The stratification patterns of other neurons and ribbon synapses were indistinguishable between wild-type and *Amigo1 KO* retinas (Fig. 4*I*–*L*). Rod bipolar cell dendrites did not extend into the outer nuclear layer, indicating that the earlier targeting errors of horizontal cell axons in *Amigo1 KO* mice do not mislead them.

AMIGO1 transmits signals for axon growth and laminar targeting

AMIGO1 could act as a receptor (i.e., transmitting signals to the cell that expresses it), as a ligand (i.e., eliciting signals in other cells), or both. To distinguish between these alternatives, we generated mice in which horizontal cells produce the RNA-guided endonuclease Cas9 (*Cx57-iCre R26-LSL-Cas9* mice; Platt et al., 2014; Hirano et al., 2016). We created adeno-associated viruses that express a single-guide RNA targeting *Amigo1* and a fluorescent reporter (*AAV2/1-U6-sgAmigo1-CAG-tdTomato*). With this AAV-CRISPR strategy, we found that *Amigo1* deletion in a small subset of horizontal cells phenocopies the selective axon deficits observed in *Amigo1 KO* mice. The size of axons of infected horizontal cells was reduced, and some branches strayed into the outer nuclear layers (Fig. 5*A*–*C*), whereas the number of dendritic and axonal synapses and the size of horizontal cell dendrites was unchanged (Fig. 5*D*–*H*). These findings indicate that AMIGO1 promotes axon growth and laminar targeting of the cells that express it (i.e., it acts as a receptor). We tried but failed to restore AMIGO1 expression via AAVs in *Amigo1 KO* mice. Thus, we cannot confirm that AMIGO1 acts as a ligand, but given its homophilic interaction profile, we think this is likely the case (Kuja-Panula et al., 2003).

Territory matching of rod bipolar cell dendrites in *Amigo1 KO* mice

Circuit function depends on the ratios in which synaptic partners are combined, which in turn depends on the relative size of their neurite arbors. Whether arbor territories of synaptic partners are actively matched and by what mechanisms is unknown. Horizontal cell axons form tripartite synapses with rod bipolar cell dendrites and rod spherules (Hoon et al., 2014; Kerschensteiner, 2020). We sparsely labeled rod bipolar cells by intravitreal injections of *AAV-Grm6-tdTomato* (Johnson et al., 2017). Rod bipolar cell dendrites were smaller in *Amigo1 KO* than wild-type mice

←

retinas, grouped by mice, sorted by size, and their averages ($\boldsymbol{K_2}$, ± SEM). ***L***, Static nonlinearities of all OFF ganglion cells recorded in wild-type ($\boldsymbol{L_1}$, left) and *Amigo1 KO* ($\boldsymbol{L_1}$, right) retinas, grouped by mice, sorted by threshold, and their averages ($\boldsymbol{L_2}$, ± SEM). ***M–R***, Cumulative probability distributions of the time to peak (***M***, wild type vs *Amigo 1KO*, $p = 0.57$, bootstrapping) and biphasic index (***N***, $p = 0.10$, bootstrapping) of temporal receptive fields, size of spatial receptive fields (***O***, $p = 0.25$, bootstrapping), and the nonlinearity (***P***, $p = 0.45$, bootstrapping), gain (***Q***, $p = 0.37$, bootstrapping), and threshold (***R***, $p = 0.37$, bootstrapping) of the effective-contrast-response functions. ns indicates $p \geq 0.05$.

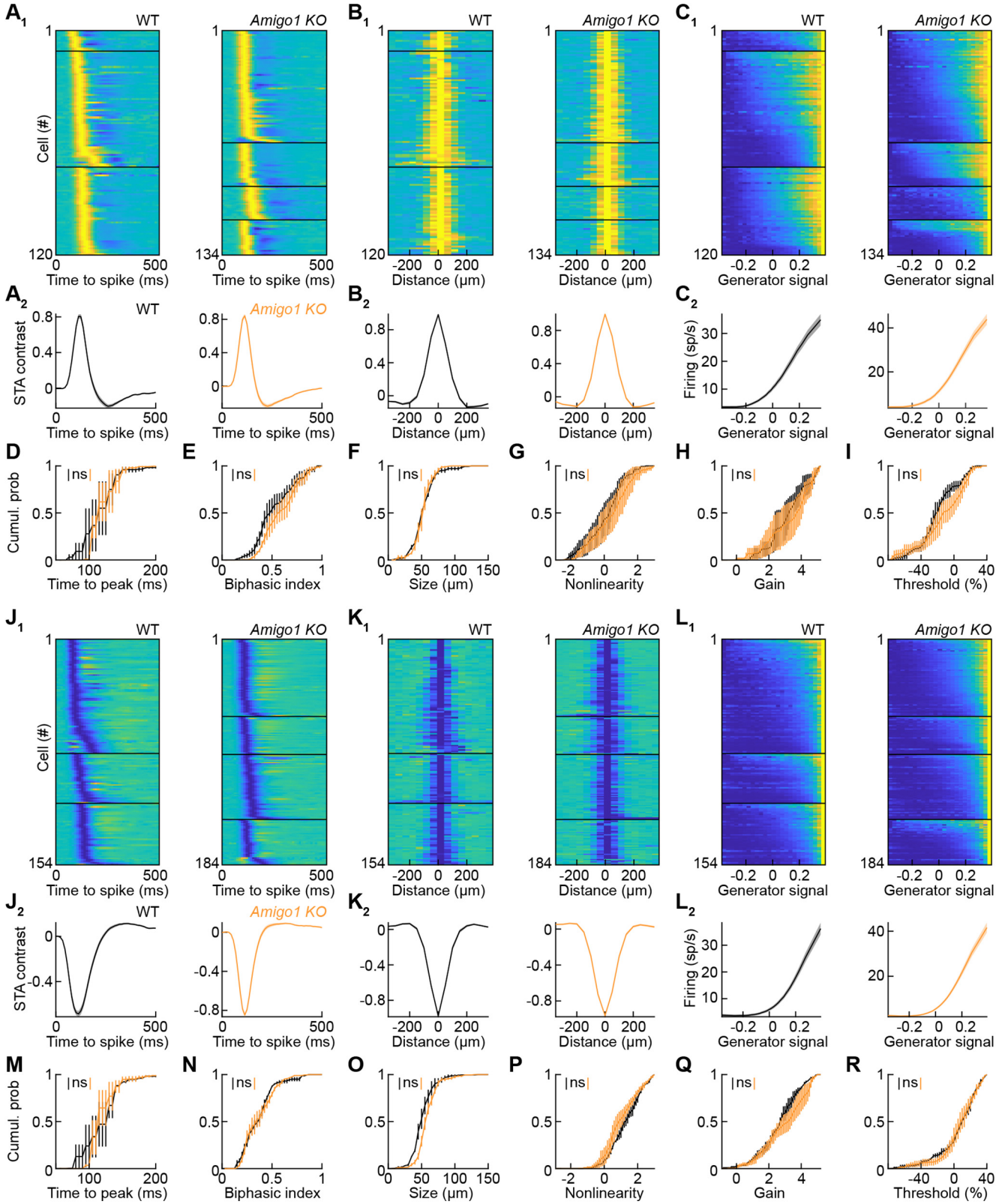

Figure 11. Homeostasis of bright-light visual processing in *Amigo1 KO* retinas. ***A***, Temporal receptive fields of all ON ganglion cells recorded in wild-type (***A*$_1$**, left, $n = 120$ cells, $n = 3$ mice) and *Amigo1 KO* (***A*$_1$**, right, $n = 134$ cells, $n = 4$ mice) retinas, grouped by mice, sorted by time to peak, and their averages (***A*$_2$**, ± SEM). ***B***, Spatial receptive fields of all ON ganglion cells recorded in wild-type (***B*$_1$**, left) and *Amigo1 KO* (***B*$_1$**, right) retinas, grouped by mice, sorted by size, and their averages (***B*$_2$**, ± SEM). ***C***, Static nonlinearities (or effective-contrast-response functions) of all ON ganglion cells recorded in wild-type (***C*$_1$**, left) and *Amigo1 KO* (***C*$_1$**, right) retinas, grouped by mice, sorted by threshold, and their averages (***C*$_2$**, ± SEM). ***D–I***, Cumulative probability distributions of the time to peak (***D***, wild type vs *Amigo 1KO*, $p = 0.76$, bootstrapping) and biphasic index (***E***, $p = 0.35$, bootstrapping) of temporal receptive fields, size of spatial receptive fields (***F***, $p = 0.66$, bootstrapping), and the nonlinearity (***G***, $p = 0.73$, bootstrapping), gain (***H***, $p = 0.68$, bootstrapping), and threshold (***I***, $p = 0.38$, bootstrapping) of the effective-contrast-response functions. ***J***, Temporal receptive fields of all OFF ganglion cells recorded in wild-type (***J*$_1$**, left, $n = 154$ cells, $n = 3$ mice) and *Amigo1 KO* (***J*$_1$**, right, $n = 184$ cells, $n = 4$ mice) retinas, grouped by mice, sorted by time to peak, and their averages (***J*$_2$**, ± SEM). ***K***, Spatial receptive fields of all OFF ganglion cells recorded in wild-type (***K*$_1$**, left) and *Amigo1 KO* (***K*$_1$**, right)

(Fig. 6*A–C*), whereas the density of their connections with rods was unchanged (Fig. 6*D*). In addition, rod bipolar cell axon size was unaffected by *Amigo1* deletion (Fig. 6*E–H*). Thus, AMIGO1, which is not expressed in rod bipolar cells, selectively promotes the growth of their dendrites to match the arbor territories of their synaptic partners.

Rods develop independently of AMIGO1

To test whether transsynaptic effects of AMIGO1 extend to rods, we sparsely labeled them by *in vivo* electroporation of *pNrl-EGFP* (Matsuda and Cepko, 2007). The density of rods and their spherule sizes were indistinguishable between *Amigo1 KO* and wild-type retinas (Fig. 7*A–D*), and, in both genotypes, rod spherules invariably had single synaptic ribbons (data not shown) opposite horizontal cell axon tips (Fig. 7*E*,*F*). Thus, the transsynaptic effects of AMIGO1 are specific to rod bipolar cells, and the presynaptic development of rods is independent of AMIGO1.

Functional homeostasis in *Amigo1 KO* retinas

The rod bipolar pathway mediates vision in dim light. In the rod bipolar pathway, horizontal cell axons provide negative feedback to rods, which send feedforward signals to the inner retina via rod bipolar cells. We hypothesized that matching adjustments of horizontal cell axon and rod bipolar cell dendrite territories serve to stabilize the rod bipolar pathway function. We recorded *in vivo* ERGs from Amigo1 KO mice and wild-type littermates to test this hypothesis. The dark-adapted a- and b-waves, reflecting rod and rod bipolar cell responses, respectively, were unaffected by *Amigo1* deletion (Fig. 8*A*,*B*). Similarly, the light-adapted b-waves, which measure cone bipolar cell responses to bright stimuli, were indistinguishable between *Amigo1 KO* and wild-type mice (Fig. 8*C*,*D*).

In addition to AMIGO1, AMIGO2 is expressed in the rod bipolar pathway (Soto et al., 2019). To test whether compensatory actions of AMIGO2 cause the functional homeostasis in *Amigo1 KO* retinas, we generated *Amigo1 Amigo2* double knockout (*DKO*) mice. Dark-adapted a- and b-waves and light-adapted a-waves did not differ significantly between *DKO* mice and wild-type littermates (Fig. 9*A–D*), indicating that the functional homeostasis of the rod bipolar pathway is independent of AMIGO2.

To probe whether the functional homeostasis extends to the output of the retina, we recorded the light responses of retinal ganglion cells on multielectrode arrays. We presented white noise stimuli at light levels preferentially activating the rod bipolar pathway (mean intensity: 10 rhodopsin isomerizations per rod per second, 10 R*, intensity range 0–20 R*; Murphy and Rieke, 2006; Pearson and Kerschensteiner, 2015) and analyzed ganglion cell responses using an LN model (Pearson and Kerschensteiner, 2015; Soto et al., 2020). The LN model consists of a linear spatiotemporal filter (i.e., the receptive field) followed by a static nonlinearity that transforms the filtered stimuli (i.e., the effective stimulus contrast) into spike responses. We separated ON and OFF ganglion cells based on their positive and negative contrast preference, respectively (Fig. 10).

The temporal and spatial receptive field components of the ON ganglion cells were indistinguishable between *Amigo1 KO* and wild-type retinas (Fig. 10*A*,*B*,*D–F*). Their effective contrast responses did not differ significantly in nonlinearity, gain, or threshold (Fig. 10*C*,*G–I*). Similarly, the spatial and temporal receptive field components and static nonlinearities of OFF ganglion cells remained stable in the face of *Amigo1* deletion (Fig. 10*J–R*). To test whether functional homeostasis in dim light comes at the expense of the bright-light function of the retina, we next presented white noise stimuli that activate cone pathways (mean intensity, 1000 R*; intensity range, 0–2000 R*). Contrast encoding of ON and OFF ganglion cells at these light levels was unchanged in *Amigo1 KO* compared with wild-type retinas (Fig. 11). Thus, the matching adjustments of horizontal cell axon and rod bipolar cell dendrite territories appear to stabilize retinal function in dim light without deteriorating retinal function in bright light.

Discussion

Here, we discover that horizontal cells express the LRR-domain cell adhesion molecule AMIGO1, which regulates their axon arbor size and, trans-synaptically, rod bipolar cell dendrite growth. AMIGO1 was first identified in a screen for molecules promoting neurite growth in cultured hippocampal neurons (Kuja-Panula et al., 2003), indicating that its function might be conserved across neuron types. AMIGO1 joins a growing list of cues that guide the assembly of the rod bipolar pathway in the outer retina (Hoon et al., 2014; Martemyanov and Sampath, 2017). The rod bipolar pathway mediates all vision near the threshold and is critical for survival, particularly in nocturnal species like mice (Field et al., 2005). The resulting selection pressure forged the complex molecular machinery that builds and maintains the rod bipolar pathway.

AMIGO1 promotes horizontal cell axon growth (Figs. 3, 5), whereas NGL2 constrains it (Soto et al., 2013, 2018). AMIGO1 interacts homophilically and likely transmits signals between neighboring horizontal cells (i.e., homotypic interactions; Kuja-Panula et al., 2003). In contrast, NGL2 on horizontal cell axon tips interacts with NTNG2 in rod spherules (i.e., trans-synaptic interactions; Soto et al., 2013, 2018). In other retinal circuits, homotypic interactions limit arbor growth, and transsynaptic interactions promote it (Lee et al., 2011; Lefebvre et al., 2015; Johnson et al., 2017; Soto et al., 2019). In this arrangement, encounters with new synaptic partners sustain arbor growth, which is slowed or altogether stopped when arbors encroach on territories of their neighbors, stabilizing the coverage of synaptic partners by a neuron population (i.e., fixed coverage). In contrast, horizontal cell axons are encouraged to grow by their neighbors (via AMIGO1) and slow as they reach their synaptic quota. This arrangement stabilizes the number of input or output synapses per neuron (i.e., fixed convergence or divergences). Sensitivity to low light is the crucial rod bipolar pathway function and depends directly on

←

retinas, grouped by mice, sorted by size, and their averages (K_2, ± SEM). ***L***, Static nonlinearities of all OFF ganglion cells recorded in wild-type (L_1, left) and *Amigo1 KO* (L_1, right) retinas, grouped by mice, sorted by threshold, and their averages (L_2, ± SEM). ***M–R***, Cumulative probability distributions of the time to peak (***M***, wild type vs *Amigo 1KO*, $p = 0.64$, bootstrapping) and biphasic index (***N***, $p = 0.56$, bootstrapping) of temporal receptive fields, size of spatial receptive fields (***O***, $p = 0.12$, bootstrapping), and the nonlinearity (***P***, $p = 0.33$, bootstrapping), gain (***Q***, $p = 0.31$, bootstrapping), and threshold (***R***, $p = 0.82$, bootstrapping) of the effective-contrast-response functions. ns indicates $p \geq 0.05$.

convergence (Dunn et al., 2006). This may explain why some mechanisms that control arbor size in the rod bipolar pathway (e.g., AMIGO1) prioritize convergence over coverage, and additional mechanisms maintain input homeostasis (Johnson et al., 2017).

Horizontal cell axons provide negative feedback to rods, which feed signals forward to rod bipolar cell dendrites (Thoreson and Mangel, 2012). The strength of the negative feedback depends on the horizontal cell axon size. The strength of rod bipolar cell responses depends on the number of rods contacted by their dendrites and the strength of rod responses (Dunn et al., 2006; Thoreson and Mangel, 2012). Thus, horizontal cell axon size and rod bipolar cell dendrite size are functionally linked. Here, we find that rod bipolar cell dendrites shrink (~83% of wild type) in parallel to horizontal cell axons (~80% of wild type) in *Amigo1 KO* mice (Fig. 6). Rod bipolar cells do not express AMIGO1. Therefore, territory matching of rod bipolar cell dendrites and horizontal cell axons is mediated by heterophilic interactions of AMIGO1 or transcellular complexes not involving AMIGO1 that sense horizontal cell axon size. AMIGO1 can interact with AMIGO2 (Kuja-Panula et al., 2003). Rod bipolar cells express AMIGO2, but their dendrites expand in *Amigo2 KO* mice (Soto et al., 2019). Thus, trans-synaptic interactions between AMIGO1 and AMIGO2 are unlikely to mediate territory matching. The extent to which territory matching generalizes to other retinal pathways and circuits previously in the nervous system remains to be tested.

References

Brown KM, Gillette TA, Ascoli GA (2008) Quantifying neuronal size: summing up trees and splitting the branch difference. Semin Cell Dev Biol 19:485–493.

Care RA, Anastassov IA, Kastner DB, Kuo Y-M, Della Santina L, Dunn FA (2020) Mature retina compensates functionally for partial loss of rod photoreceptors. Cell Rep 31:107730.

Chapot CA, Behrens C, Rogerson LE, Baden T, Pop S, Berens P, Euler T, Schubert T (2017) Local signals in mouse horizontal cell dendrites. Curr Biol 27:3603–3615.e5.

Chattopadhyaya B, Di Cristo G, Higashiyama H, Knott GW, Kuhlman SJ, Welker E, Huang ZJ (2004) Experience and activity-dependent maturation of perisomatic GABAergic innervation in primary visual cortex during a postnatal critical period. J Neurosci 24:9598–9611.

Chichilnisky EJ (2001) A simple white noise analysis of neuronal light responses. Network 12:199–213.

Crandall SR, Cox CL (2012) Local dendrodendritic inhibition regulates fast synaptic transmission in visual thalamus. J Neurosci 32:2513–2522.

Diamond JS (2017) Inhibitory interneurons in the retina: types, circuitry, and function. Annu Rev Vis Sci 3:1–24.

Dunn FA, Doan T, Sampath AP, Rieke F (2006) Controlling the gain of rod-mediated signals in the Mammalian retina. J Neurosci 26:3959–3970.

Euler T, Detwiler PB, Denk W (2002) Directionally selective calcium signals in dendrites of starburst amacrine cells. Nature 418:845–852.

Field GD, Sampath AP, Rieke F (2005) Retinal processing near absolute threshold: from behavior to mechanism. Annu Rev Physiol 67:491–514.

Grimes WN, Zhang J, Graydon CW, Kachar B, Diamond JS (2010) Retinal parallel processors: more than 100 independent microcircuits operate within a single interneuron. Neuron 65:873–885.

Hasan N, Ray TA, Gregg RG (2016) CACNA1S expression in mouse retina: novel isoforms and antibody cross-reactivity with GPR179. Vis Neurosci 33:E009.

Hirano AA, Liu X, Boulter J, Grove J, Pérez de Sevilla Müller L, Barnes S, Brecha NC (2016) Targeted deletion of vesicular GABA transporter from retinal horizontal cells eliminates feedback modulation of photoreceptor calcium channels. eNeuro 3:ENEURO.0148-15.2016.

Hoon M, Okawa H, Della Santina L, Wong ROL (2014) Functional architecture of the retina: development and disease. Prog Retin Eye Res 42:44–84.

Hsiang J-C, Johnson KP, Madisen L, Zeng H, Kerschensteiner D (2017) Local processing in neurites of VGluT3-expressing amacrine cells differentially organizes visual information. Elife 6:e31307.

Huckfeldt RM, Schubert T, Morgan JL, Godinho L, Di Cristo G, Huang ZJ, Wong ROL (2009) Transient neurites of retinal horizontal cells exhibit columnar tiling via homotypic interactions. Nat Neurosci 12:35–43.

Johnson RE, Tien N-W, Shen N, Pearson JT, Soto F, Kerschensteiner D (2017) Homeostatic plasticity shapes the visual system's first synapse. Nat Commun 8:1220.

Kerschensteiner D (2020) Mammalian retina development. In: The senses: a comprehensive reference (Fritzsch B, ed), pp 234–251. Oxford: Elsevier.

Kuja-Panula J, Kiiltomäki M, Yamashiro T, Rouhiainen A, Rauvala H (2003) AMIGO, a transmembrane protein implicated in axon tract development, defines a novel protein family with leucine-rich repeats. J Cell Biol 160:963–973.

Lee SCS, Cowgill EJ, Al-Nabulsi A, Quinn EJ, Evans SM, Reese BE (2011) Homotypic regulation of neuronal morphology and connectivity in the mouse retina. J Neurosci 31:14126–14133.

Lefebvre JL, Sanes JR, Kay JN (2015) Development of dendritic form and function. Annu Rev Cell Dev Biol 31:741–777.

Leinonen H, Pham NC, Boyd T, Santoso J, Palczewski K, Vinberg F (2020) Homeostatic plasticity in the retina is associated with maintenance of night vision during retinal degenerative disease. Elife 9:e59422.

Li CH, Lee CK (1993) Minimum cross entropy thresholding. Pattern Recognit 26:617–625.

Martemyanov KA, Sampath AP (2017) The transduction cascade in retinal ON-bipolar cells: signal processing and disease. Annu Rev Vis Sci 3:25–51.

Matsuda T, Cepko CL (2007) Controlled expression of transgenes introduced by *in vivo* electroporation. Proc Natl Acad Sci U S A 104:1027–1032.

Matsuda T, Cepko CL (2008) Analysis of gene function in the retina. Methods Mol Biol 423:259–278.

Morgan JL, Lichtman JW (2020) An individual interneuron participates in many kinds of inhibition and innervates much of the mouse visual thalamus. Neuron 106:468–481.e2.

Murphy GJ, Rieke F (2006) Network variability limits stimulus-evoked spike timing precision in retinal ganglion cells. Neuron 52:511–524.

Nelson R, von Litzow A, Kolb H, Gouras P (1975) Horizontal cells in cat retina with independent dendritic systems. Science 189:137–139.

Pearson JT, Kerschensteiner D (2015) Ambient illumination switches contrast preference of specific retinal processing streams. J Neurophysiol 114:540–550.

Platt RJ, Chen S, Zhou Y, Yim MJ, Swiech L, Kempton HR, Dahlman JE, Parnas O, Eisenhaure TM, Jovanovic M, Graham DB, Jhunjhunwala S, Heidenreich M, Xavier RJ, Langer R, Anderson DG, Hacohen N, Regev A, Feng G, Sharp PA, et al. (2014) CRISPR-Cas9 knockin mice for genome editing and cancer modeling. Cell 159:440–455.

Prigge CL, Kay JN (2018) Dendrite morphogenesis from birth to adulthood. Curr Opin Neurobiol 53:139–145.

Reese BE, Keeley PW (2015) Design principles and developmental mechanisms underlying retinal mosaics. Biol Rev Camb Philos Soc 90:854–876.

Rodieck RW (1991) The density recovery profile: a method for the analysis of points in the plane applicable to retinal studies. Vis Neurosci 6:95–111.

Schindelin J, Arganda-Carreras I, Frise E, Kaynig V, Longair M, Pietzsch T, Preibisch S, Rueden C, Saalfeld S, Schmid B, Tinevez J-Y, White DJ, Hartenstein V, Eliceiri K, Tomancak P, Cardona A (2012) Fiji: an open-source platform for biological-image analysis. Nat Methods 9:676–682.

Shen N, Wang B, Soto F, Kerschensteiner D (2020) Homeostatic plasticity shapes the retinal response to photoreceptor degeneration. Curr Biol 30:1916–1926.e3.

Sher A, Jones BW, Huie P, Paulus YM, Lavinsky D, Leung L-SS, Nomoto H, Beier C, Marc RE, Palanker D (2013) Restoration of retinal structure and function after selective photocoagulation. J Neurosci 33:6800–6808.

Sinha R, Hoon M, Baudin J, Okawa H, Wong ROL, Rieke F (2017) Cellular and Circuit Mechanisms shaping the perceptual properties of the primate fovea. Cell 168:413–426.e12.

Soto F, Watkins KL, Johnson RE, Schottler F, Kerschensteiner D (2013) NGL-2 regulates pathway-specific neurite growth and lamination, synapse formation, and signal transmission in the retina. J Neurosci 33:11949–11959.

Soto F, Zhao L, Kerschensteiner D (2018) Synapse maintenance and restoration in the retina by NGL2. Elife 7:e30388.

Soto F, Tien N-W, Goel A, Zhao L, Ruzycki PA, Kerschensteiner D (2019) AMIGO2 scales dendrite arbors in the retina. Cell Rep 29:1568–1578.e4.

Soto F, Hsiang J-C, Rajagopal R, Piggott K, Harocopos GJ, Couch SM, Custer P, Morgan JL, Kerschensteiner D (2020) Efficient coding by midget and parasol ganglion cells in the human retina. Neuron 107:656–666.e5.

Szikra T, Trenholm S, Drinnenberg A, Jüttner J, Raics Z, Farrow K, Biel M, Awatramani G, Clark DA, Sahel J-A, da Silveira RA, Roska B (2014) Rods in daylight act as relay cells for cone-driven horizontal cell-mediated surround inhibition. Nat Neurosci 17:1728–1735.

Thoreson WB, Mangel SC (2012) Lateral interactions in the outer retina. Prog Retin Eye Res 31:407–441.

Trümpler J, Dedek K, Schubert T, de Sevilla Müller LP, Seeliger M, Humphries P, Biel M, Weiler R (2008) Rod and cone contributions to horizontal cell light responses in the mouse retina. J Neurosci 28:6818–6825.

Valenzuela DM, Murphy AJ, Frendewey D, Gale NW, Economides AN, Auerbach W, Poueymirou WT, Adams NC, Rojas J, Yasenchak J, Chernomorsky R, Boucher M, Elsasser AL, Esau L, Zheng J, Griffiths JA, Wang X, Su H, Xue Y, Dominguez MG, et al. (2003) High-throughput engineering of the mouse genome coupled with high-resolution expression analysis. Nat Biotechnol 21:652–659.

Van Rossum G, Drake FL (2009) Python 3 reference manual. Scotts Valley, CA: CreateSpace.